Rare Metal Materials and Engineering
Volume 54, Issue 4, April 2025
Available online at www.rmme.ac.cn

Science Press

Cite this article as: Yu Lei, Cao Rui, Ma Jinyuan, et al. Effects of Thermal Aging on Microstructure and Mechanical Properties of Interface of Hot Isostatic Pressing Densified Low Alloy Steel with Inconel 690 Cladding[J]. Rare Metal Materials and Engineering, 2025, 54(04): 879-885. DOI: https://doi.org/10.12442/j.issn.1002-185X.20240100.

ARTICLE

Effects of Thermal Aging on Microstructure and Mechanical Properties of Interface of Hot Isostatic Pressing Densified Low Alloy Steel with Inconel 690 Cladding

Yu Lei[1,2], Cao Rui[1,2], Ma Jinyuan[1,2], Yan Yingjie[1,2], Dong Hao[3,4], Wang Caiqin[3,4]

[1] State Key Laboratory of Advanced Processing and Recycling of Nonferrous Metals, Lanzhou University of Technology, Lanzhou 730050, China; [2] School of Materials Science and Engineering, Lanzhou University of Technology, Lanzhou 730050, China; [3] Advanced Technology & Materials Co., Ltd, Beijing 100081, China; [4] Hebei Hot Isostatic Pressing Technology Innovation Center, Zhuozhou 072750, China

Abstract: The microstructure, micro-hardness, and tensile properties of interface between hot isostatic pressing densified low alloy steel and Inconel 690 cladding were investigated during the aging process at 600 °C. The results show that the interface region can be divided into four zones from base metal to deposited metal: carbon-depleted zone (CDZ), partial melting zone (PMZ), planar growth zone (PGZ), and brownish feature zone (BFZ). Dimensions of these zones do not significantly change during aging. However, type I carbides noticeably increase in size in the PMZ, and precipitates clearly occur in the PGZ. The main reason for their growth and occurrence is continuous carbon migration. The highest micro-hardness appears in the PGZ and BFZ regions, which is related to carbon accumulation and precipitates in these regions. Tensile failure occurs on the base metal side due to the high strength mismatch between these two materials. The CDZ, composed of only ferrite, has lower strength and fractures at the boundary between CDZ and base metal. The ultimate tensile strength decreases by only 50 MPa after aging for 1500 h, and the interface region maintains high strength without significant deformation.

Key words: interface; thermal aging; microstructure; mechanical properties; hot isostatic pressing densification

1 Introduction

Ni-based alloy claddings on steel are usually used in oil, petrochemical, nuclear, and marine industries, owing to their excellent wear, corrosion, and high-temperature oxidation resistance[1–4]. High-quality claddings are essential for long-term security service. However, Ni-based alloys are prone to various welding defects, like solidification cracking[5–6], liquid cracking[6–7], ductility-dip cracking[8–9], strain-age cracking[10], and pores[11]. To reduce these defects, several methods have been developed, such as welding method optimization[12–13], welding and heat treatment parameter adjustment[14–15], rare earth element addition[16], and hot isostatic pressing (HIP) densification[17].

HIP densification has been proven to be an effective method for repairing welding defects in Ni-based alloys[18]. However, most studies have focused on densification parameters and degrees[17–20], with few attention given to the interface evolution, especially interface microstructure and mechanical properties evolution under thermal conditions. Ni-based alloy/steel interfaces have complex microstructures and are susceptible to premature failure. Zhang et al[21] showed that the formation and propagation of oxide resulted in interfacial failure of the Inconel 617/9Cr steel under creep conditions. Choi et al[22] found that Cr carbides were enhanced by thermal aging near the interface. They also found that galvanic corrosion occurred near the interfaces of both alloy 152/low alloy steel and alloy 182/low alloy steel[23]. Kim et al[24] determined that thermal aging increases the susceptibility to stress corrosion cracking of Ni-based alloy/low alloy steel

Received date: April 25, 2024
Foundation item: Major Scientific and Technological Project of Gansu (22ZD6GA008); Excellent Doctorate Project of Gansu (23JRRA806); National Natural Science Foundation of China (52175325, 51961024, 52071170)
Corresponding author: Cao Rui, Ph. D., Professor, School of Materials Science and Engineering, Lanzhou University of Technology, Lanzhou 730050, P. R. China, E-mail: caorui@lut.edu.cn

interface. Therefore, a fundamental understanding of the unique microstructure and mechanical properties of interface is essential to improve the insights into the degradation and failure behavior.

Microstructure and mechanical properties are key parameters affecting materials degradation and failure. Also, accelerated thermal aging is required to investigate the thermal aging effect on the interface[22]. To investigate the effect of thermal aging on Ni-based alloy/low alloy steel integrity, the present research analyzed the microstructure and mechanical property evolution of the interface between Inconel 690 and low alloy steel after HIP densification and thermal aging through optical microscope (OM), scanning electron microscope (SEM), micro-hardness test, and tensile test.

2 Experiment

Fig. 1 illustrates the schematic of Inconel 690 cladding preparation and subsequent treatment. The base metal was Q345B low alloy steel with 30 mm in thickness. Inconel 690 wire with 1 mm in diameter was used as the deposited metal. Their nominal chemical composition is provided in Table 1. The surface of the base metal was firstly ground to remove the oxide layer and then cleaned with acetone, alcohol, and other organic solvents to ensure optimal surface conditions.

The cladding was performed using gas tungsten arc welding to produce a layer with a minimum thickness of 15 mm. The overlap ratio of each pass was approximately 30%, and all subsequent passes were conducted at an inter-pass temperature of 170 ℃. Specific welding parameters are listed in Table 2.

No post-weld heat treatment was performed after the cladding process. The cladding component was subjected to HIP densification at 1120 ℃ under 150 MPa for 2 h, and then cooled in a furnace.

To investigate the evolution of microstructure and mechanical properties of the interface under thermal conditions, some HIP densified specimens were subjected to thermal aging treatment at 600 ℃ (below the phase transition temperature of low alloy steel) for 0–1500 h. Specimens aged for 100, 200, 500, 1000, and 1500 h were selected to analyze the evolution of microstructure, micro-hardness, and tensile properties.

The joint was ground with 600#, 800#, 1000#, 1500#, 2000#, and 3000# sand papers and polished with diamond particles (0.25 μm), and then some of the specimens were electrolytically etched by 10% chromic acid solution to observe the microstructure of the deposited metal. While others were etched by 4% nital to reveal the microstructure of the base metal. Microstructural characteristics were investigated by OM and SEM coupled with energy-dispersive spectroscope (EDS).

Micro-hardness and tensile tests were conducted to evaluate the mechanical property evolution of the joint during aging. For micro-hardness test, a PG-2 type micro-hardness testing machine was used, with a force of 10 N applied for 15 s. To ensure reliable results, ten tests were performed for each specimen along the fusion boundary. The reported micro-hardness was obtained by averaging the results measured at surface displacements of 200 μm for each indentation. The tensile tests were carried out using a universal testing machine at a speed of 0.008 mm/s. Because the thickness of the cladding layer was only 13 mm, the non-standard tensile specimens were machined and their schematic diagram is shown in Fig.1.

3 Results and Discussion

3.1 Microstructure of HIP densified interface

Fig.2a shows OM micrograph of the HIP densified interface on the base metal side. The microstructure far away from the fusion boundary consists of typical ferrite and pearlite, while

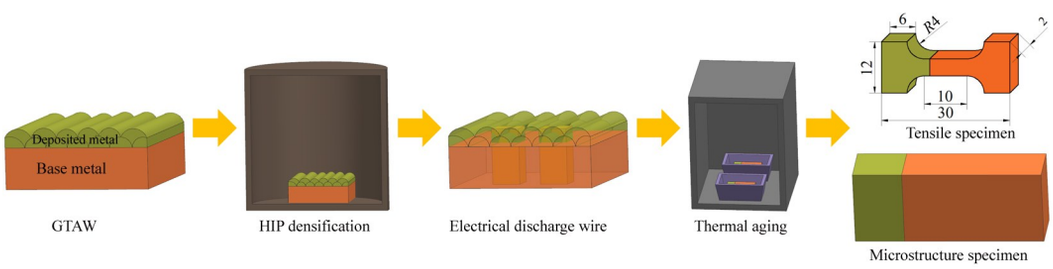

Fig.1 Schematic of Inconel 690 cladding preparation and subsequent treatment

Table 1 Chemical composition of deposited metal and base metal (wt%)

Material	Cr	Fe	Ni	Si	Ti	Al	Mn	C
Inconel 690	27.41	9.50	Bal	0.19	0.38	0.69	0.72	0.06
Low alloy steel	0.022	Bal	0.01	0.22	0.0008	0.012	1.21	0.16

Table 2 Specific welding parameters for cladding

Current/A	Wire feed rate/cm·min^{-1}	Welding speed/cm·min^{-1}	Gas flow rate/L·min^{-1}	Wire feed angle/(°)
160	100	15	15	70–75

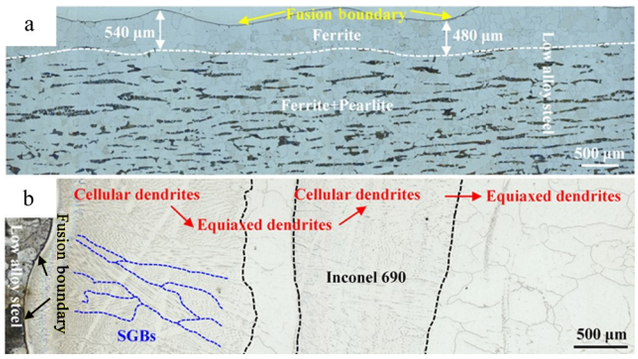

Fig.2 OM micrographs of HIP densified interface: (a) base metal and (b) deposited metal

the microstructure close to the fusion boundary is composed of ferrite with a grain size of several tens of microns. This result is caused by cementite dissolution at about 500 μm from the fusion boundary and carbon diffusion from the base metal to the deposited metal. Hence, this region is sometimes referred to as the carbon-depleted zone (CDZ) or decarburized zone[25–27].

Fig. 2b displays OM micrograph of the HIP densified interface on the deposited metal side, in which SGBs refer to solidification grain boundaries. The bottom of the first welding layer and the second layer mainly exhibits cellular dendrites with large elongated grains, which are millimeter-sized in the welding solidification direction, and several hundred microns in the transversal section. Meanwhile, the surface of the first welding layer and the second layer mainly exhibits equiaxed structures with several hundred microns of grains.

To investigate the interface microstructure, a high-magnification OM micrograph was analyzed, as shown in Fig. 3a. A white layer of about 10 μm without any obvious features is revealed, and it exhibits planar grains. After that, the grains change to cellular grains far away from the fusion boundary. This transformation is related to changes in its solidification modes during welding, and is controlled by temperature gradient in the liquid (G_L), solidification growth rate (R), and composition[28]. Heterogeneous nucleation of a solid substrate is called epitaxial nucleation. When the composition of the substrate and liquid is similar, the solidification front that grows from a given grain on that substrate will retain the same crystallographic orientation. Since grain orientation of the substrate is generally random, this results in a continuation of the crystallographic misorientation of the base metal grains across the fusion boundary into the solidifying solid. Consequently, grain boundaries are continuous across the original fusion boundary where epitaxial nucleation occurs. In fcc and bcc metals, solidification growth occurs preferentially along the cube edge, or <100> crystallographic directions, which are sometimes called “easy growth” directions, since solidification is the most efficient in crystallographic orientation, as shown in Fig.3b[28–30].

Fig. 4 shows SEM micrograph and corresponding EDS result of the HIP densified interface. The interface from base metal to deposited metal can be divided into CDZ, partial melting zone (PMZ), and partially mixed zone. The CDZ is composed of ferrite according to the OM micrograph analysis in Fig.1. The PMZ is the actual fusion boundary in Fig.1 and is about 5 μm in width, as shown in Fig. 4a. From the magnified micrograph and the EDS result of this region, as shown in Fig. 5, it is clear that the PMZ is rich in carbon compared to CDZ and the planar growth zone (PGZ), and exhibits type I and type II carbide morphologies, which are commonly reported in Ni-based alloy/steel interface after high temperature long-term service[31–33]. The partially mixed zone is divided into two zones according to the SEM morphology: PGZ and brownish feature zone (BFZ). These zones are separated by planar grain boundaries. The PGZ appears as a bright band (about 10 μm) in Fig.3a and lacks distinct features in Fig. 4a. The BFZ, located at the deposited metal side adjacent to the PGZ, reveals a markedly different morphology in Fig. 4a. According to the research of LAS/Alloy 52 by Akhatova et al[27], nano-sized $M_{23}C_6$ precipitates are observed in the BFZ, and no thermodynamically predicted Cr_7C_3 carbides are found in the PGZ. This finding provides a plausible explanation for the morphological difference between the PGZ and the BFZ in Fig.4a. Consistent with the composition given in Table 1, a compositional gradient exists between the base metal and deposited metal. Fig.4b shows a distinct intermediate zone with substitutional content gradients, inferring a compositional transition region. Fe, Ni,

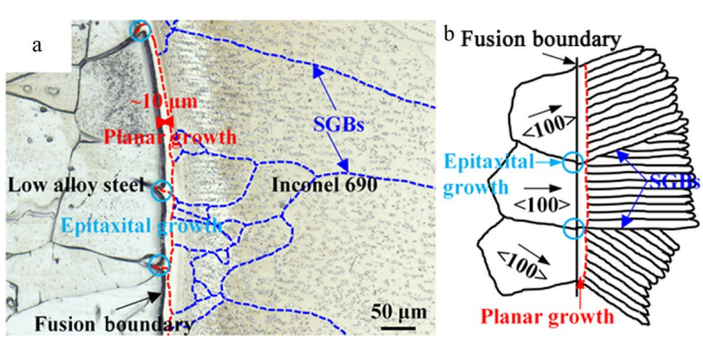

Fig.3 High-magnification OM micrograph of the interface region (red line: boundary of the planar growth; blue line: SGBs; light blue circle: epitaxial growth) (a); schematic of epitaxial nucleation mechanism (b)[28]

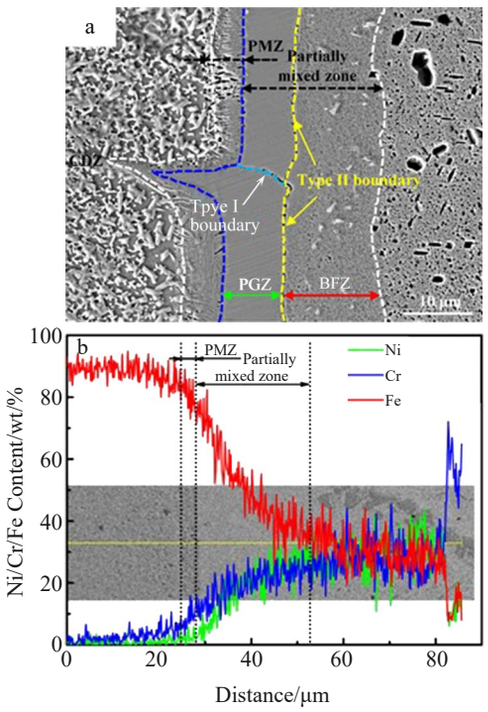

Fig.4 SEM micrograph (a) and corresponding EDS line scanning results (b) of the HIP densified interface

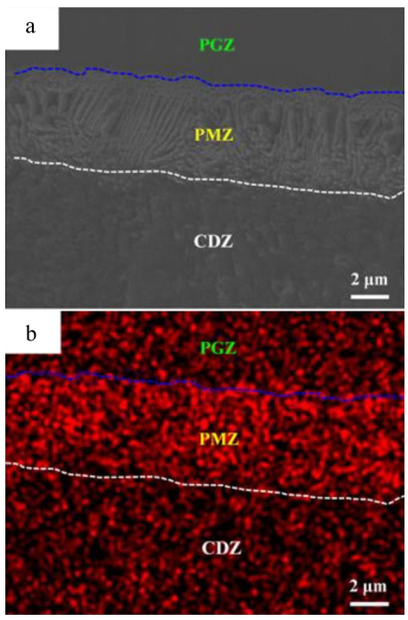

Fig.5 SEM micrograph (a) and corresponding EDS mapping of element C (b) of the HIP densified interface (CDZ)

and Cr contents change gradually across the PMZ, PGZ, and BFZ, and the transition distance is about 20 μm.

3.2 Evolution of microstructure during aging

The joint was subjected to thermal aging for 100, 200, 500, 1000, and 1500 h. The microstructure of the interface was analyzed by SEM, as shown in Fig. 6. It can be observed that the PMZ, PGZ, and BFZ have dimensions similar to those in Fig. 4a, without obvious change during the aging process. However, morphologies of the PMZ and the PGZ after aging are significantly different from the HIP densified morphologies, especially after aging for 1500 h, as shown in Fig. 7a. Larger type I carbides appear in the PMZ, with a slight increment of 1–2 μm in width. In Fig. 7b, needle-shaped precipitates occur in the PGZ, which are not present in the HIP densified specimen. This phenomenon may be attributed to carbon migration and carbide precipitation during the aging process.

3.3 Evolution of mechanical properties during aging

To evaluate evolution of mechanical property of the joint during the aging process, both micro-hardness and tensile properties of the joint were examined. Fig. 8 illustrates the micro-hardness evolution of the interface region during aging.

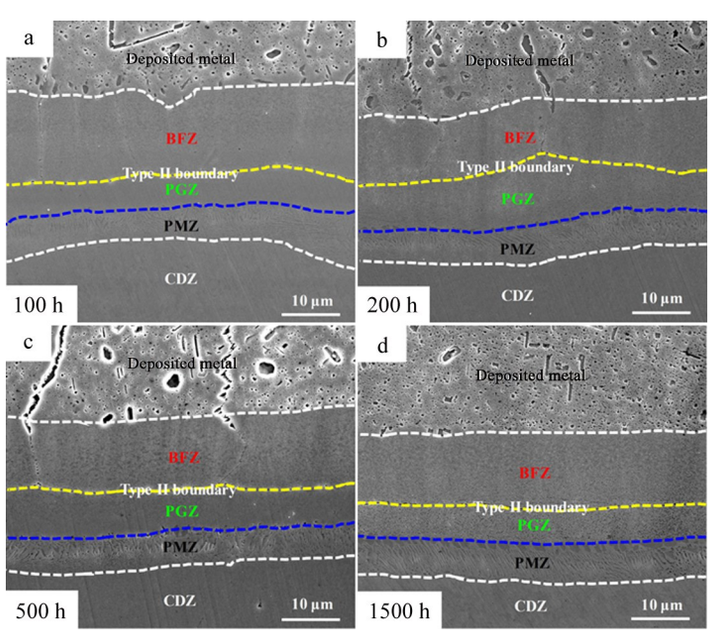

Fig.6 SEM micrographs of interface after thermal aging for different durations: (a) 100 h, (b) 200 h, (c) 500 h, and (d) 1500 h

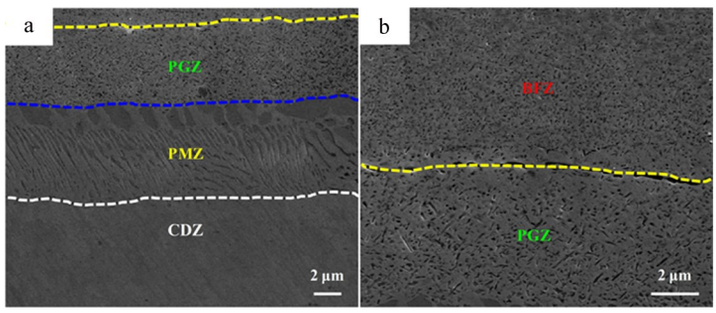

Fig.7 SEM micrographs of interface after aging for 1500 h: (a) PMZ and PGZ; (b) PGZ and BFZ

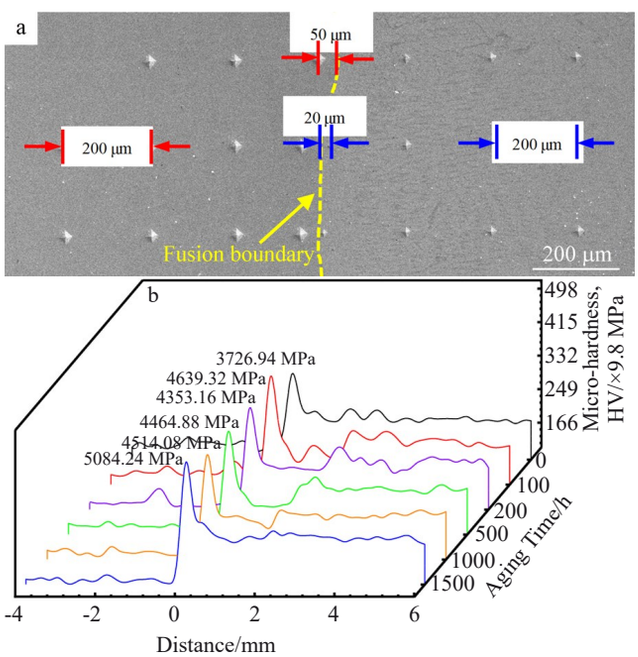

Fig.8 Micro-hardness of HIP densified and aged interface: (a) location of indentations in the interface region; (b) micro-hardness evolution during aging

The higher micro-hardness appears at the deposited metal side. No significant difference occurs between the HIP densified and aged specimens except for the first point of the deposited metal. The first point of the deposited metal, located in the region between PGZ and BFZ, has the highest micro-hardness, as observed in Fig. 8a. This specific region exhibits more pronounced micro-hardness changes compared to other regions. After aging for 100 h, the micro-hardness increases from 3726.94 MPa to 4639.32 MPa and remains essentially constant during aging for 200, 500, and 1000 h. The micro-hardness reaches 5084.24 MPa after aging for 1500 h, which is the highest value obtained in this work, as shown in Fig.8b.

Fig.9 illustrates the evolution of ultimate tensile strength of the joint. It is observed that the strength slightly decreases with aging time, and after aging for 1500 h, it is about 50 MPa lower than that of the HIP densified specimens. The failure occurs on the base metal side, exhibiting obvious plastic deformation, as shown in the inserts in Fig. 10. Fig. 10 demonstrates the evolution of the interface region after tensile

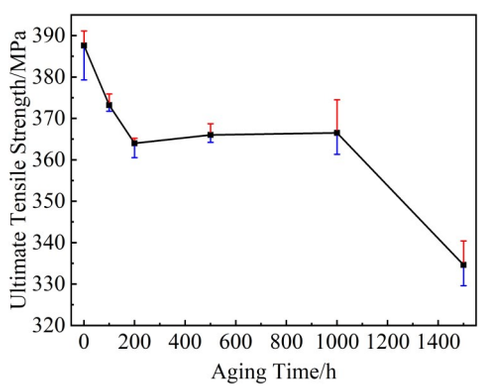

Fig.9 Evolution of ultimate tensile strength of the joint during aging process

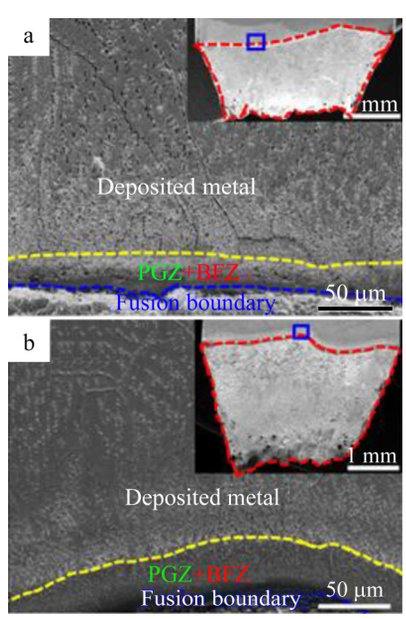

Fig.10 SEM micrographs of HIP densified (a) and 1500 h-aged (b) interfaces after tensile test (insets show morphology of fracture profile)

testing. No significant plastic deformation is observed on the deposited metal side for all specimens. However, serious deformation occurs on the base metal side along the interface. This phenomenon indicates that the deposited metal does not reach its yield stress during tensile test. The large strength

difference between the deposited metal and the base metal leads to yielding in the base metal firstly. Meanwhile, The CDZ is composed of only ferrite, rather than ferrite and pearlite for the base metal. These two reasons cause necking occurring at the boundary between CDZ and base metal. The decrement of 50 MPa in strength suggests that aging has a small influence on the tensile strength, and the interface regions retains higher strength than the base metal.

3.4 Interface microstructure evolution during aging

The interface region can be classified into four distinct zones from the base metal to the deposited metal, which are CDZ, PMZ, PGZ, and BFZ. The PMZ is identified as fusion boundary in OM images (Fig. 1–Fig. 3) due to low magnification, and reveals a band (5–8 μm in width) rich in carbon with type I and/or type II carbide morphologies in SEM images (Fig. 4–7). SEM and EDS results in Fig. 5 show that lath type II carbides with a high carbon content clearly appear in the PMZ. After aging for 1500 h, carbides, especially the spheroidicity type I carbides, significantly grow, as shown in Fig. 7a. These results are consistent with Parker's[31] research that type I carbides grow with aging time at 625 °C. The PGZ with 10 μm in width is adjacent to the fusion boundary, and it is also referred to as "featureless zone" by Dai et al[34–35]. This zone has no obvious precipitates in the HIP densified condition, as shown in Fig. 4a. However, after aging, evident needle-shaped M_7C_3 carbides appear in this zone, as reported by Dodge's researches[36–37]. The BFZ is part of the deposited metal cellular grains adjacent to the PGZ, and precipitates in this zone are different from the deposited metal, as shown in Fig. 6. TEM results have confirmed that the precipitates in the BFZ are nano-sized $M_{23}C_6$ carbides[27].

Based on the microstructure observation of the interface region, the bonding between the base metal and the deposited metal is attributed to the epitaxial growth mechanism. The melted weld metal nucleates along the grain boundaries of base metal and rapidly solidifies into planar crystals during the welding solidification process. Due to quick solidification rate, the precipitated phases do not have sufficient time to form, resulting in the formation of "featureless zone". After planar growth, the solidification rate decreases but remains high, resulting in the formation of BFZ, where nano-sized $M_{23}C_6$ precipitates are observed. As the solidification rate further decreases, larger precipitates form in the cellular grains. Carbides in the PGZ and BFZ increase after aging, particularly in the PGZ after aging for 1500 h. It is attributed to the aging temperature promoting carbon migration from the base metal to the deposited metal, resulting in a high carbon solution at high temperatures. As the temperature gradually decreases, the carbon solution also decreases, leading to the precipitation of carbides M_7C_3 and $M_{23}C_6$ in the PGZ and the BFZ, respectively.

3.5 Property evolution of interface region

The PGZ and BFZ combined region exhibit the highest micro-hardness value, which is consistent with the results in previous studies[12,34,38]. The micro-hardness of this region increases from 3726.94 MPa to 4639.32 MPa after 100 h of aging and remains nearly constant after aging for 200, 500, and 1000 h, indicating that precipitates have precipitated in this region and the balance between the number and size of precipitates results in the stable micro-hardness in subsequent processes. After aging for 1500 h, the micro-hardness increases significantly to 5084.24 MPa due to continuous carbon migration and a greater number of precipitates in the PGZ and BFZ, as reported by Ref.[15,27,35–37].

Tensile tests show that the interface region is not the weakest zone. The failure occurs on the base metal side with significant plastic deformation. In contrast, after tensile test, no obvious deformation occurs on the deposited metal side, including the PGZ and the BFZ, indicating higher yield stress compared to the base metal. During the tensile process, yield phenomena first appear at the base metal, while the deposited metal is remained in the elastic process. The deformation hardening of the base metal cannot reach the yield stress of the deposited metal, indicating a high strength mismatch between the two materials. As a result, the deformation is concentrated at the base metal side and ultimately fracture occurs from the weakest zone. The CDZ, composed of only ferrite rather than ferrite and pearlite of the base metal, has lower strength and fractures at the boundary between CDZ and base metal. The strength only decreases by 50 MPa after 1500 h of aging, indicating that aging has little influence on the tensile strength of the joint.

4 Conclusions

1) Interface of the joint can be divided into CDZ, PMZ, PGZ, and BFZ zones from the base metal to the deposited metal. Due to carbon migration and cementite dissolution, the CDZ consists of only ferrite rather than ferrite and pearlite in the base metal, and the grain size is obviously larger than that of the base metal. The PMZ shows a band (5–8 μm in width) with type I and/or type II carbides. The PGZ shows a 10 μm epitaxial growth band from the PMZ, which has featureless for the HIP densified specimen. However, obvious precipitates occur after thermal aging. The BFZ is part of the deposited metal cellular grains adjacent to the PGZ, with much smaller precipitates than those of the deposited metal.

2) The continuous carbon migration and more precipitates in PGZ and BFZ result in higher micro-hardness, which increases from 3726.94 MPa to 5084.24 after aging for 1500 h.

3) Tensile strength of the joint is slightly decreased by 50 MPa after aging, and fractures occur in the base metal. The large difference between the two materials leads to the base metal yielding firstly, and subsequent deformation hardening cannot reach the yield strength of the deposited metal. Cementite dissolves in the CDZ, leading to the lowest strength and resulting in fracture at the boundary of the CDZ and the base metal.

References

1 Huang J, Liu S, Yu S *et al. Journal of Manufacturing Processes*[J], 2020, 56: 106

2 Liu Q B, Liu Z D, Wang Y T *et al. Rare Metal Materials and*

Engineering[J], 2023, 52(4): 1210
3 Wu Jinjiang, Zhao Guangdi, Wang Bo *et al. Materials China*[J], 2024, 43(10): 902 (in Chinese)
4 Zareie R H R, Akbari M S A A. *Materials Science and Engineering A*[J], 2012, 556: 454
5 Wang Dan, Kadoi Kota, Yamamoto Motomichi *et al. Rare Metal Materials and Engineering*[J], 2021, 50(7): 2435 (in Chinese)
6 Guo Yang, Zhang Jianxun, Xiong Jiankun *et al. Rare Metal Materials and Engineering*[J], 2021, 50(4): 1462 (in Chinese)
7 Aqeel M, Shariff S M, Gautam J P *et al. Materials and Manufacturing Processes*[J], 2021, 36: 904
8 Rapetti A, Christien F, Tancret F *et al. Scripta Materialia*[J], 2021, 194: 113680
9 Chen J, Zhang P, Mo T *et al. Science and Technology of Welding and Joining*[J], 2021, 26(4): 294
10 Zhang G, Xiao C, Taheri M. *Journal of Manufacturing Processes*[J], 2020, 52: 66
11 Chiang M F, Chen C. *Materials Chemistry and Physics*[J], 2009, 114: 415
12 Ming H, Zhang Z, Wang J *et al. Materials Characterization*[J], 2017, 123: 233
13 Frei J, Alexandrov B T, Rethmeier M. *Welding in the World*[J], 2018, 62: 317
14 Xu F J, Lv Y H, Xu B S *et al. Materials & Design*[J], 2013, 45: 446
15 Liu F C, Nelson T W, McCracken S L. *Metallurgical and Materials Transactions A*[J], 2019, 50(6): 2826
16 Saida K, Taniguchi A, Okauchi H *et al. Science and Technology of Welding and Joining*[J], 2013, 16(6): 553
17 Hsu K T, Wang H S, Chen H G *et al. Metals*[J], 2016, 6(10): 238
18 Xie J, Ma Y, Xing W *et al. Welding in the World*[J], 2018, 62: 471
19 Sentyurina Z A, Baskov F A, Loginov P A *et al. Additive Manufacturing*[J], 2021, 37: 101629
20 Tillmann W, Schaak C, Nellesen J *et al. Additive Manufacturing*[J], 2017, 13: 93
21 Zhang Y, Li K, Cai Z *et al. Materials Science and Engineering A*[J], 2019, 764: 138185
22 Choi K J, Kim J J, Lee B H *et al. Journal of Nuclear Materials*[J], 2013, 441: 493
23 Choi K J, Yoo S C, Kim S *et al. Corrosion Science*[J], 2019, 153: 138
24 Kim J, Kim S H, Choi K J *et al. Corrosion Science*[J], 2014, 86: 295
25 Lindqvist S, Ahonen M, Lydman J *et al. Engineering Fracture Mechanics*[J], 2019, 214: 320
26 Ming H, Zhang Z, Wang J *et al. Materials Characterization*[J], 2019, 148: 100
27 Akhatova A, Robaut F, Verdier M *et al. Materials Science and Engineering A*[J], 2020, 788: 139592
28 Lippold J C. *Welding Metallurgy Principles, Welding Metallurgy and Weldability*[M]. New York: John Wiley & Sons, 2014: 9
29 Ranjbar K, Dehmolaei R, Amra M *et al. Welding in the World*[J], 2018, 62(6): 1121
30 Devendranath R K, Arivazhagan N, Narayanan S. *Materials & Design*[J], 2012, 40: 70
31 Parker J D, Stratford G C. *Journal of Materials Science*[J], 2000, 35: 4099
32 Nicholso R D. *Metals Technology*[J], 1984, 11: 115
33 Li Kejian, Li Xiaogang, Zhang Yu *et al. Electric Welding Machine*[J], 2020, 50(9): 17 (in Chinese)
34 Dai T, Lippold J C. *Journal of Materials Engineering and Performance*[J], 2018, 27(7): 3411
35 Dai T, Lippold J C. *Welding in the World*[J], 2018, 62(3): 535
36 Dodge M F, Dong H B, Gittos M F. *Materials Research Innovations*[J], 2014, 18(S4): 907
37 Dodge M F. *The Effect of Heat Treatment on the Embrittlement of Dissimilar Welded Joints*[D]. Leicester: University of Leicester, 2014
38 Dong L, Peng Q, Xue H *et al. Corrosion Science*[J], 2018, 132: 9

时效对热等静压致密化低合金钢上堆焊Inconel 690界面组织及性能的影响

余　磊[1,2]，曹　睿[1,2]，马金元[1,2]，闫英杰[1,2]，董　浩[3,4]，王彩芹[3,4]
(1. 兰州理工大学 省部共建有色金属先进加工与再利用国家重点实验室，甘肃 兰州 730050)
(2. 兰州理工大学 材料科学与工程学院，甘肃 兰州 730050)
(3. 安泰科技股份有限公司，北京 100081)
(4. 河北热等静压技术创新中心，河北 涿州 072750)

摘　要：在600 ℃时效处理过程中，对热等静压致密化处理的低合金钢上堆焊Inconel 690界面微观结构、显微硬度和拉伸性能进行了研究。结果表明，从基体到堆焊层，界面区域可以分为4个区：贫碳区（CDZ）、局部熔化区（PMZ）、平面生长区（PGZ）和棕色特征区（BFZ）。这些区域的尺寸在时效过程中没有显著变化。然而，I型碳化物在PMZ中明显增大，而在PGZ中出现明显沉淀。它们长大和出现的主要原因是时效过程中连续的碳迁移。界面最高显微硬度出现在PGZ和BFZ区域，这与该区域中碳的堆积和沉淀有关。由于这2种材料之间较高的强度不匹配性，拉伸失效发生在基体侧。由于CDZ仅由铁素体组成，强度较低，断裂通常发生在CDZ和基体的界面处。在经过1500 h的时效处理后，抗拉伸强度仅降低了50 MPa，并且界面区域保持高强度且无明显变形。

关键词：界面；时效；组织；力学性能；热等静压致密化

作者简介：余　磊，男，1995年生，博士生，兰州理工大学材料科学与工程学院，甘肃 兰州 730050，E-mail：yuleilut@outlook.com